Surface Functionalization of Semiconductor and Oxide Nanocrystals with Small Inorganic Oxoanions (PO_4^{3-}, MoO_4^{2-}) and Polyoxometalate Ligands

Jing Huang,[†] Wenyong Liu,[†] Dmitriy S. Dolzhnikov,[†] Loredana Protesescu,[‡,§] Maksym V. Kovalenko,[‡,§] Bonil Koo,[⊥] Soma Chattopadhyay,[∥] Elena V. Shenchenko,[⊥] and Dmitri V. Talapin[†,⊥,*]

[†]Department of Chemistry and James Franck Institute, University of Chicago, Chicago, Illinois 60637, United States, [‡]Department of Chemistry and Applied Biosciences, Laboratory for Inorganic Chemistry, ETH Zurich, CH-8006 Zurich, Switzerland, [§]EMPA — Swiss Federal Laboratories for Materials Science and Technology, CH-8600 Dübendorf, Swizterland, [⊥]Center for Nanoscale Materials, Argonne National Laboratory, Argonne, Illinois 60439, United States, and [∥]CSRRI-IIT, MRCAT, APS, Argonne National Laboratory, and Physics Department, Illinois Institute of Technology, 3300 South Federal Street, Chicago, Illinois 60616, United States

ABSTRACT In this work, we study the functionalization of the nanocrystal (NC) surface with inorganic oxo ligands, which bring a new set of functionalities to all-inorganic colloidal nanomaterials. We show that simple inorganic oxoanions, such as PO_4^{3-} and MoO_4^{2-}, exhibit strong binding affinity to the surface of various II—VI and III—V semiconductor and metal oxide NCs. ζ-Potential titration offered a useful tool to differentiate the binding affinities of inorganic ligands toward different NCs. Direct comparison of the binding affinity of oxo and chalcogenidometallate ligands revealed that the former ligands form a stronger bond with oxide NCs (*e.g.*, Fe_2O_3, ZnO, and TiO_2), while the latter prefer binding to metal chalcogenide NCs (*e.g.*, CdSe). The binding between NCs and oxo ligands strengthens when moving from small oxoanions to polyoxometallates (POMs). We also show that small oxo ligands and POMs make it possible to tailor NC properties. For example, we observed improved stability upon Li^+-ion intercalation into the films of Fe_2O_3 hollow NCs when capped with MoO_4^{2-} ligands. We also observed lower overpotential and enhanced exchange current density for water oxidation using Fe_2O_3 NCs capped with $[P_2Mo_{18}O_{62}]^{6-}$ ligands and even more so for $[\{Ru_4O_4(OH)_2(H_2O)_4\}(\gamma\text{-}SiW_{10}O_{36})_2]$ with POM as the capping ligand.

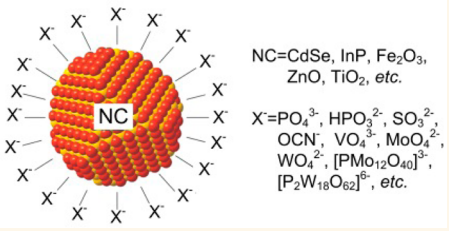

KEYWORDS: nanocrystals · surface chemistry · inorganic ligands · oxoanion ligands · polyoxometalate ligands · water oxidation · Li-ion battery

Recent developments in nanomaterial synthesis have introduced reliable synthetic pathways toward nanosized colloidal forms of various metals, semiconductors, magnets, catalysts, and other functional materials.[1−3] The ability to precisely control the size and shape of such inorganic nanocrystals (NCs) and nanoparticles introduces new ways to fine-tune material properties and cointegrate dissimilar components to form multifunctional systems.[4−9] The majority of colloidal synthesis methods use high temperatures and nonpolar high-boiling organic solvents. These routes allow obtaining highly crystalline monodisperse NCs that have surfaces decorated with organic ligands (*e.g.*, oleic acid, hexadecylamine, trioctylphosphine oxide, *etc.*) containing long hydrocarbon chains. These ligands are perfectly suitable for dispersing NCs in nonpolar solvents (hexane, toluene, *etc.*) or in organic polymers. At the same time, the highly insulating nature of organic surface ligands leads to serious limitations for most solid-state device applications (photovoltaics, electronics, thermoelectrics, *etc.*) of colloidal NCs. Furthermore, surface ligands determine access to and the activity of catalytic centers at the NC surface. Organic ligands also make it difficult to integrate colloidal nanoparticles with other inorganic materials, *e.g.*, with ceramics made by sol—gel chemistry.[10,11]

The introduction of inorganic surface ligands[12] opened up new opportunities for

* Address correspondence to dvtalapin@uchicago.edu.

Received for review June 25, 2014 and accepted August 24, 2014.

Published online August 24, 2014
10.1021/nn503458y

applications of nanomaterials. Recent works showed high electron mobility, high photoconductivity, or enhanced thermoelectric performance in inorganically capped NC assemblies.[13−19] These developments have also resulted in the integration of colloidal NCs into inorganic hosts, such as chalcogenide glasses.[20] All-inorganic nanocrystals are typically obtained by exchanging organic surface ligands with molecular metal chalcogenide complexes (MCCs)[12] or metal-free anionic species such as S^{2-} and SCN^-.[21,22] These NCs capped with inorganic ligands are soluble in polar solvents such as water, dimethylformamide (DMF), or formamide (FA). Halide, pseudohalide, and halometallate ligands have recently been shown to stabilize colloidal NCs.[23,24] It was also shown that organic ligands could be removed by using ligand-stripping agents such as $NOBF_4$, HBF_4, or Me_3OBF_4.[21,25,26] These agents helped cleave the NC−ligand bonds forming "naked" positively charged NCs charge-balanced by weakly nucleophilic tetrafluoroborate anions.

Inorganic NCs attract significant attention for various applications, including solution-processed semiconductors, lithium-ion battery materials, catalysts for water splitting, oxygen reduction reactions (ORR), and so forth. These applications require new surface modifications, including efficient interfacing with oxides or high chemical stability characteristics of oxides. For instance, oxo ligands can be useful for the integration of engineered nanomaterials into amorphous metal oxide hosts for building new composites, as recently shown by the Milliron group for indium tin oxide NCs capped with polyniobate POMs as precursors for obtaining glasses with electrochromic properties.[27] Over a decade ago, the Finke group used POMs for the synthesis of transition metal nanoparticles.[28−31] In this report, we describe a comprehensive study on the use of small oxoanions, such as PO_4^{3-}, MoO_4^{2-}, as capping agents. We also outline the general ligand exchange strategy, which is applicable for oxidatively stable NCs, such as iron oxides, and for materials that require additional care to prevent oxidation and etching (*e.g.*, CdSe). We compare the results with more established MCC ligands. We show that the binding affinity of different oxoanions to the NCs surface is closely related to solvent pH and other reaction parameters, and also follows the basic principles of hard and soft acid−base interactions, that is, the higher affinity of oxoligands to harder cations.

In this work, we not only provide a generalized methodology of the organic-to-oxoanion ligand exchange, but we also illustrate potential applications of this surface chemistry for electrochemical conversion and storage of energy. The combination of functional metallic, magnetic, or semiconducting nanocrystals and POMs with rich redox chemistry represents an interesting opportunity for the rational design of multifunctional materials and catalytic systems. Recently, the Cummings group reported that CO_2 can bind MoO_4^{2-}. Attaching these moieties to the NC surface may open an opportunity to use MoO_4^{2-} ligands as binding pockets for the photo- or electrochemical reduction of CO_2.[32] The combination of quantum dots and catalytically active polyoxometallates through chemical bondings can form efficient, microscopic reaction centers for the water splitting reaction. We therefore compare small oxoanions with selected examples of catalytically active polyoxometalates (*e.g.*, $K_6[P_2W_{18}O_{62}]$, $K_6[P_2Mo_{18}O_{62}]$, $Rb_8K_2[\{Ru_4O_4(OH)_2(H_2O)_4\}(\gamma\text{-}SiW_{10}O_{36})_2]$). All these applications require an understanding of the binding affinity of different inorganic oxo ligands to the NC surface.

RESULTS AND DISCUSSION

Two-Step Exchange of Original Organic Ligands with Oxoanions. Generally, oxo ligands are less nucleophilic than MCCs, and attaching them to the NC surface can be challenging. Unlike our previous studies on MCCs or metal-free chalcogenide ligands,[12,21,33] most of the oxoanions did not replace the organic ligands on the surface of NCs directly through a phase transfer procedure. So we conducted a two-step procedure that included removal of the original covalently bound organic ligands followed by the attachment of inorganic ligands to ligand-free NC surfaces.

Murray *et al.* recently reported a generalized ligand exchange procedure using nitrosonium tetrafluoroborate ($NOBF_4$) to remove the organic ligands from the NC surface, resulting in nearly ligand-free positively charged NCs, which can be dispersed in DMF, dimethyl sulfoxide (DMSO) or acetonitrile (ACN).[25] This approach worked well for Fe_2O_3, FePt, Bi_2S_3, and $NaYF_4$ NCs but not for CdSe and other semiconductor NCs, primarily because of the oxidation of chalcogenide NCs by NO^+.[25] We later reported that tetrafluoroboric acid (HBF_4) or hexafluorophosphoric acid (HPF_6) can efficiently remove organic ligands from CdSe NCs.[21] H^+ cleaved the bond between Cd atoms and surface ligands leaving behind unbound positively charged metal sites on the NC surface.[21] $NOBF_4$ can be easily hydrolyzed by traces of water present in NC solution generating HBF_4 in the reaction $NOBF_4 + H_2O \rightarrow HNO_2 + HBF_4$. Both $NOBF_4$ and HBF_4 result in a very acidic environment that may etch NCs, limiting their applications as general ligand-removal agents.[25,26]

Helms *et al.* further improved this procedure by introducing trialkyloxonium salts, such as $Me_3O^+BF_4^-$, that reacted with DMF solvent producing an efficient alkylating agent $[Me_2N{=}CH(OMe)]^+BF_4^-$ that worked as relatively mild nonoxidizing and less acidic ligand stripping agent.[26,34] In the present work we show that triphenylcarbenium tetrafluoroborate ($Ph_3C^+BF_4^-$) can be also used as an efficient ligand-stripping agent for colloidal NCs (Figure S1, Supporting Information

(SI)). In analogy with the ligand stripping mechanism for HBF_4,[21] where H^+ acted as electrophile to cleave the Cd−O or Cd−N surface-ligand bonds, Ph_3C^+ is a very strong electrophile capable of removing organic ligands. It efficiently stripped ligands off the surfaces of Fe_2O_3 and CdSe NCs. The oxidation potential of $Ph_3C^+BF_4^-$ ($E^0 = -0.11$ V in MeCN *vs* ferrocene) is much smaller compared to that of $NOBF_4$ ($E^0 = 0.87$ V in MeCN *vs* ferrocene).[35] In addition, compared to all previously used ligand-stripping agents, Ph_3C^+ is strongly hydrophobic, which provided an additional convenience for separating the reaction products from the NCs dispersed in a highly polar solvent, like FA.

The completeness of the surface organic ligand removal with all four ligand-stripping agents was studied using FTIR spectra (Figure S2 (SI)). It showed that the majority of surface organic ligands had been removed: the C−H vibration bands at 2500−3000 cm^{-1} were strongly suppressed. Among the four ligands stripping agents, $NOBF_4$ and HBF_4 removed the organic ligands most completely, which might be explained by the acidic etching of the NC surface. We also noticed that removing organic ligands by treating precipitated NCs with $NOBF_4$ or HBF_4 was less efficient compared with a direct phase transfer of colloidal NCs from a nonpolar to polar solvent. In the former case, we always observed some organic residue showing C−H vibrations from 2700−3500 cm^{-1} (Figure S2 (SI)). As prepared CdSe, InP, and Fe_2O_3 NCs showed positive ζ-potential in DMF after organic ligands were removed using $Me_3O^+BF_4^-$ or HBF_4. The positive ζ-potential indicated the presence of charged metal sites on the NC surface (Figure S3 (SI)). These NCs were charge-balanced with BF_4^-, known as a very weak nucleophile, acting as counterions without specific binding to the NC surface.[36]

We want to emphasize the critical role of pH for successful functionalization of inorganic NCs with oxo ligands. The pH scale was originally introduced as a measure of acid−base equilibria in aqueous solutions, but it can also be used for nonaqueous media.[37] According to IUPAC Recommendations 2002, 0.05 mol kg^{-1} of potassium hydrogen phthalate (KHPh) solution is used as the most fundamental pH buffer having reference pH values assigned to it.[37] The pH values in a particular organic solvent can be correlated to the aqueous pH scale through the following expression:

$$\text{pH (aqueous scale)} = \text{pH (solvent scale)} - \log \gamma_t$$

$$\gamma_t = e^{\Delta_t G_H^0/RT}$$

where $\Delta_t G_H{}^0$ is the standard molar Gibbs free energy of proton transfer from water into a given solvent.[38] For example, $\log \gamma_t$ is −3.15 in the case of DMF. We calibrated the pH glass electrode in DMF and measured the pH of CdSe and Fe_2O_3 NCs in DMF under different conditions (Table 1). For example, colloidal solutions of

TABLE 1. pH Values of CdSe NCs and Fe_2O_3 NCs Dispersed in DMF[a]

treatment	pH
CdSe-$Me_3O^+BF_4^-$-DMF	5.21
CdSe-$Ph_3C^+BF_4^-$-DMF	2.67
CdSe-HBF_4-DMF	1.60
CdSe-HBF_4-DMF (washed with DMF and toluene)	6.36 (once)
	8.87 (twice)
CdSe-HBF_4-DMF (washed with acetonitrile and FA)	11.67
Fe_2O_3-$Me_3O^+BF_4^-$-DMF	3.14
Fe_2O_3-$Ph_3C^+BF_4^-$-DMF	1.72
Fe_2O_3-$NOBF_4$-DMF	1.81
Fe_2O_3-HBF_4-DMF	1.40
Fe_2O_3-HBF_4-DMF (washed with DMF and toluene)	3.47 (once)
	7.59 (twice)
Fe_2O_3-HBF_4-DMF (washed with acetonitrile and FA)	11.07

[a] All pH values are based on the DMF pH scale.

Fe_2O_3 NCs treated with either $NOBF_4$ or HBF_4 showed strong acidity (~1.4−1.8) in DMF, while the same NCs showed a higher pH (around 3) after treatment with $Me_3O^+BF_4^-$. If we further washed Fe_2O_3 NCs treated with $NOBF_4$ or HBF_4 with FA/ACN solvent/nonsolvent combination, the pH of the solution increased to approximately 11. We found that the high pH of ligand-free NC colloidal solutions was important for successful functionalization of the NC surface with oxo ligands.

The pH of the NC solution is mostly determined by the acid introduced with the ligand-stripping agent, which can be either directly acidic as HBF_4 or it can generate acid *in situ* through hydrolysis as $NOBF_4$. In fact, $Me_3O^+BF_4^-$ can also undergo hydrolysis and generate acid in the reaction $Me_3O^+BF_4^- + H_2O \rightarrow Me_2O + MeOH + HBF_4$. The rate of hydrolysis depends on many factors including H_2O concentration, temperature, and possible catalysis by the NC surface. Additional washings with anhydrous solvents (formamide, acetonitrile, *etc.*) helped remove excess HBF_4. If acid is not removed from the NC solution, it can protonate the oxoanion or POM ligands making them unreactive. The optimal pH range should depend on the pK_a of a particular inorganic ligand in a given solvent and on the binding affinity of this ligand toward the NC surface. The upper bound of a suitable pH range is determined by the possibility of solvent deprotonation at high pH values.

Small Oxoanions As Surface Ligands for NCs. Removal of the organic ligands generated NCs with positive surface charges. In the second step of ligand exchange, NCs were mixed with negatively charged oxo ligands and dispersed in highly polar solvents such as FA or *N*-methylformamide (NMF). NMF was particularly useful because of its exceptionally high static dielectric constant $\varepsilon = 182$. It was able to stabilize most of the NCs capped with a variety of inorganic ligands.

We explored various simple oxoanions (SO_4^{2-}, SO_3^{2-}, PO_4^{3-}, HPO_3^{2-}, ClO_4^-, ClO_3^-, OCN^-, $S_2O_3^{2-}$,

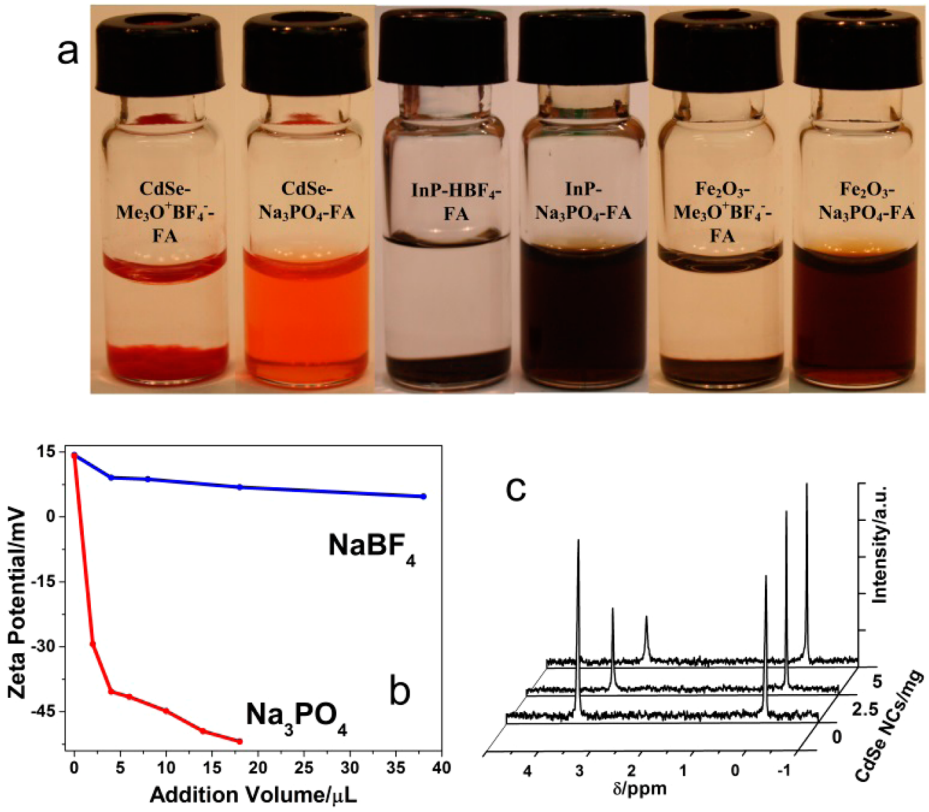

Figure 1. (a) Photographs illustrating the colloidal stability of CdSe, InP, and Fe_2O_3 in FA treated with just Me_3OBF_4 and with the subsequent addition of Na_3PO_4. (b) Evolution of the ζ-potential of CdSe NCs upon titration with $NaBF_4$ (blue) and Na_3PO_4 (red), respectively. (c) ^{31}P NMR spectra of 1.25 mg/mL of Na_3PO_4 solution in formamide with 0, 2.5, and 5 mg of CdSe NCs, respectively, from front to the back. H_3PO_4 was used as the internal standard in all three cases.

VO_4^{3-}, MoO_4^{2-}, WO_4^{2-}, *etc.*) using Fe_2O_3 and CdSe NCs as the typical examples for metal oxide and semiconductor NCs, respectively. We found that in the case of CdSe NCs, only $S_2O_3^{2-}$ (which could bind to NC through its terminal sulfur atom) and VO_4^{3-} can directly displace organic surface ligands and transfer CdSe NCs from hexane into FA phase. We performed the two-step ligand exchange procedure for other ligands. Ligand-free CdSe and Fe_2O_3 NCs were first precipitated from their stable solutions in DMF and dispersed in FA along with oxoanion ligands. It turned out that the stabilization of oxoanion-capped NCs in polar solvents was strongly dependent on the pH of the NC solution. When we used $NOBF_4$ or HBF_4 to remove organic ligands, it usually resulted in very acidic conditions in DMF or FA (pH 1−2 on the corresponding solvent scale) that were not beneficial for binding most of the oxoanion ligands to NC surfaces, most likely because of the protonation of oxoanions in solution. CdSe NCs could only be colloidally stabilized by $S_2O_3^{2-}$, while Fe_2O_3 NCs could be stabilized by VO_4^{3-}, MoO_4^{2-}, and WO_4^{2-} within this very acidic environment. To improve the ligand exchange chemistry, we further washed the NCs with FA/ACN as solvent/nonsolvent. Such additional purification increased the pH (Table 1) to a value suitable for oxoanion adsorption and reduced the ionic strength coming from excessive ions present in the solution.

The suspensions of ligand-stripped CdSe or Fe_2O_3 NCs in FA do not show long-term colloidal stability, and the addition of coordinating anionic ligands is necessary for obtaining stable colloidal solutions (Figure 1a). To explore the effect of oxoanions on the NC surface charge, we compared ζ-potentials of CdSe NCs upon addition of oxoanion or $NaBF_4$. In aqueous or similar media, a ζ-potential of ±30 mV is regarded as the borderline between stable and unstable colloids. We conducted a simplified ζ-potential titration experiment to study the ligand binding process for CdSe NCs. We measured the electrophoretic mobility (μ) of NCs, which is related to ζ-potential through the Henry equation, $\mu = (2\varepsilon_0\varepsilon_r\zeta f(\kappa r))/(3\eta)$,[39] where ε_0 is the vacuum permittivity, ε is the relative permittivity of solvent, and η is the solvent viscosity. Also, $f(\kappa r)$ is a dimensionless monotonically varying function of a particle with hydrodynamic radius r and the Debye screening parameter κ:

$$\kappa^{-1} = (\varepsilon_r\varepsilon_0 k_B T/2N_A e^2 I)^{1/2}$$

where I is the ionic strength of the solution.

$NaBF_4$ solution in DMF or FA with a concentration of 4 mM was added to all samples to define the ionic strength. Usually, for a polar solvent with a moderate

TABLE 2. Summary of Colloidal Stability for CdSe and Fe_2O_3 NCs Capped with Oxo Ligands in FA[a]

ligands	CdSe-OA	Fe_2O_3-OA	InP-MA	InP-TOP	InAs-TOP
NaOCN	−	+			
$Na_2S_2O_3$	+	−	−	−	−
Na_2SO_3	−	+			
Na_3PO_4	+	+	+	+	+
Na_3VO_4	+	+			
$NaVO_3$	+	+	+	+	+
Na_2HPO_3	+	+			
NaH_2PO_2	+	+			
Na_2WO_4	+	+	+	+	−
Na_2MoO_4	+	+	+	+	−
Na_2HAsO_4	+	+	+	+	+
$Na_3[PMo_{12}O_{40}]$			+	−	−
$K_6[P_2W_{18}O_{62}]$			−	−	−

[a] "+" corresponds to the ability of particular NCs to form stable colloidal solutions with a given oxo ligand. "−" corresponds to failed attempts to form stable colloids. A NC solution was considered stable if the solution was optically clear and did not form precipitate over weeks or under centrifugation. OA: oleic acid, MA: myristic acid, TOP: tri-*n*-octylphosphine.

ionic strength, a Smoluchowski approximation of $f(\kappa r)$=1.5 is used at $\kappa r \gg 1$ (Smoluchowski limit). However, our NC solutions, even in polar solvents, did not approach the Smoluchowski limit because of the small particle size. Therefore, we used $f(\kappa r) \approx 1$ (Huckel limit).

In general, after organic ligands removal, we considered the NCs to be "ligand-free". They were positively charged because of the unsaturated surface metal sites and showed colloidal stability in DMF, DMSO, and ACN. The addition of excessive BF_4^- anions increased the ionic strength of the solution and resulted in a gradual decrease of the ζ-potential until the NC colloid slowly lost colloidal stability (Figure 1b). This loss of colloidal stability can be explained by efficient screening of the positive charge on NCs with BF_4^- ions that weakens electrostatic repulsion between NCs in solution. On the other hand, the addition of oxoanions, like PO_4^{3-}, resulted in recharging CdSe NCs, as confirmed by the sign change of the ζ-potential (Figure 1b).

Using a very similar approach, we were able to stabilize CdSe, InP, and Fe_2O_3 NCs with VO_4^{3-}, MoO_4^{2-}, WO_4^{2-}, PO_4^{3-}, AsO_4^{3-}, HPO_3^{2-}, $H_2PO_2^-$, *etc.* in FA, as shown in Table 2 and Figure S4 (SI). Other metal oxide NCs (ZnO, $CoFe_2O_4$, and TiO_2) also formed stable colloidal solutions in the presence of different oxoanions (Figures S5 and S6 (SI)). All the metal oxide NCs could be easily dispersed into DMF after the organic ligands were removed with $NOBF_4$. The ligand chemistry of these NCs with oxoanions and POMs is summarized in Table S3 (SI). To better understand the interactions between NCs and oxo ligands, we focused on several cases and carried out comparative studies of oxoanion ligands and similar sulfur-based inorganic ligands.

PO_4^{3-} as a Ligand for CdSe, InP, and Fe_2O_3 NCs. In the case of PO_4^{3-}, stable colloids formed only at a reasonably high pH for both CdSe and Fe_2O_3 NCs. It means that when $NOBF_4$ or HBF_4 is used as the ligand-stripping agent, positively charged NCs in DMF need to be additionally washed with FA/ACN solvent/nonsolvent combination to obtain a suitable pH for PO_4^{3-} adsorption. However, ligand exchange with InP NCs can happen even at a low pH value. Positively charged InP NCs that were not additional washed were easily stabilized by PO_4^{3-} anions in FA because of a strong affinity of In^{3+} surface sites toward PO_4^{3-} ligands. Obtained solutions retained excellent colloidal stability for weeks (Figure 1a).

The nucleophilicity of PO_4^{3-} is low compared with MCC ligands and the one remaining question is what happens if PO_4^{3-} binds to the NC surface rather than assist with colloidal stabilization in some other way (*e.g.*, by changing the pH of the solution). The sign change of the ζ-potential (Figure 1b) suggested that the PO_4^{3-} anion was bound to the positive surface metal sites. We also measured ^{31}P NMR on CdSe NCs with PO_4^{3-} ligands in FA to see if we can observe direct ligand binding through NMR measurements. The sample was made of 0.4 mL of Na_3PO_4 (1.25 mg/mL) solution in FA. ^{31}P NMR spectrum of free PO_4^{3-} in FA was measured first, followed by the addition of positively charged CdSe NCs in FA, which was prepared by carefully dispersing positively charged CdSe NCs into FA with a concentration of 25 mg/mL. 0.1 mL of CdSe NCs in FA was added into the sample with each addition. The interaction of PO_4^{3-} with the NC surface is expected to produce surface-bound (immobilized) phosphate molecules with significantly broadened and attenuated NMR signals.[40] In practice, this often leads to the disappearance of the bound species from the NMR spectra of the solution. This broadening originated from the presence of large anisotropic dipolar couplings and anisotropies of chemical shifts.[41] The addition of CdSe NCs to a solution of Na_3PO_4 in FA resulted in strong suppression of the intensity of the PO_4^{3-} signal accompanied by some minor change of the phosphorus chemical shift. We normalized the phosphorus peak from the H_3PO_4 internal reference and compared the intensity of the Na_3PO_4 signals for three samples containing no CdSe NCs, 2.5 mg and 5 mg CdSe NCs (Figure 1c). Such a decrease of the phosphorus signal intensity suggested that free PO_4^{3-} ions quickly attached to the surface of CdSe NCs. The change in chemical shift by 0.6 ppm could originate from partial protonation of PO_4^{3-} due to a lower pH of the added CdSe NC solution in FA. This is a relatively small variation as compared with the overall spread of possible ^{31}P NMR chemical shifts.

The absorption spectra of CdSe NCs capped with PO_4^{3-} showed that the excitonic peaks of CdSe NCs did

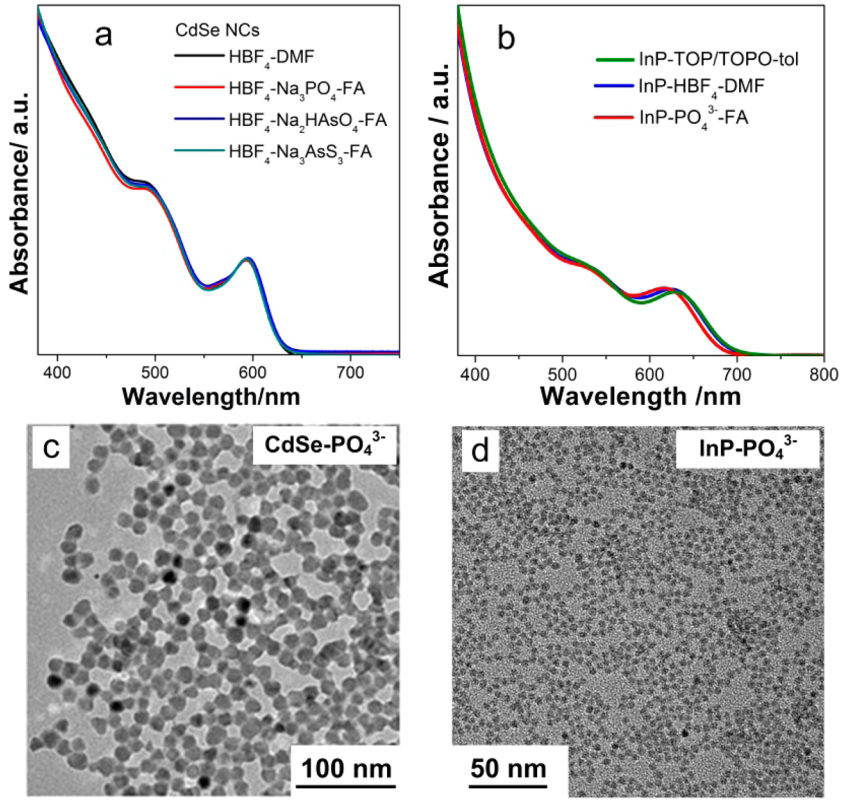

Figure 2. (a) Absorption spectra of ~4.0 nm CdSe NCs treated with HBF_4 *via* the two-step ligand exchange process with HBF_4+Na_3PO_4, HBF_4+Na_2HAsO_4, and HBF_4+Na_3AsS_3. (b) Absorption spectra of ~4.2 nm InP NCs, capped with TOP/tri-*n*-octylphosphine oxide (TOPO), treated with HBF_4 and HBF_4−Na_3PO_4, respectively. (c) TEM image of ~12 nm CdSe NCs capped with Na_3PO_4 ligands. (d) TEM image of 4.2 nm InP NCs capped with Na_3PO_4 ligands.

not shift after the ligand exchange procedure was performed. Similar behavior was observed for CdSe NCs capped with AsS_3^{3-} and $HAsO_4^{2-}$ ligands, showing that the NC cores stayed intact during surface functionalization (Figure 2a). Very similar behavior has been observed for III−V NCs (InP) and oxide NCs (Fe_2O_3). The same approach can be used with core−shell NCs, *e.g.*, CdSe/CdS. Figure 2c,d shows typical TEM images of PO_4^{3-}-capped CdSe and InP NCs, respectively. ICP-OES elemental analysis was used to estimate the numbers of PO_4^{3-} ligands attached per NC. 4 nm CdSe NCs (containing ~620 CdSe units) and 10 nm Fe_2O_3 (containing ~10000 Fe_2O_3 units) bonded approximately 135 and 325 PO_4^{3-} ligands, respectively. Tables S1 and S2 (SI) summarize the elemental composition for CdSe and Fe_2O_3 NCs stabilized with different oxo ligands.

MoO_4^{2-}-Capped CdSe and Fe_2O_3 NCs. In this subsection, we show characteristic features of molybdate MoO_4^{2-} ions as capping ligands and compare them with structurally similar MoS_4^{2-} MCCs. For CdSe NCs, MoS_4^{2-} can easily replace surface organic ligands through a direct phase transfer procedure, as described in other work by our group.[12] At the same time, for CdSe NCs originally capped with oleic acid (OA)/oleylamine (OLA)/TOP, ligand exchange with MoO_4^{2-} needed a mediated two-step ligand exchange procedure. Additional washing with FA/ACN was necessary if HBF_4 was used as the ligand-stripping agent. In the case of OA-capped Fe_2O_3 NCs, neither MoS_4^{2-} nor MoO_4^{2-} can replace the surface organic ligands through a direct phase transfer procedure.

Figure 3a compares the adsorption spectra of CdSe NCs before and after ligand exchange with MoS_4^{2-} or MoO_4^{2-} ligands. The samples were freshly prepared in a glovebox to prevent possible oxidation. The first excitonic peak showed almost no changes after ligand exchange, indicating that CdSe NCs retained their mean size and monodispersity. Very similar behavior was observed for InP NCs. The strong suppression of N−H and C−H vibrations coming from organics around 2700−3500 cm^{-1} was seen in the FTIR spectra acquired for CdSe NCs before and after ligand exchange with MoS_4^{2-} or MoO_4^{2-}. It confirms that the majority of the surface organic ligands were removed after ligand exchange (Figure S7 (SI)), which is similar to the behavior observed for MCC ligands. The absorption band at 3100−3500 cm^{-1} of $(NH_4)_2MoS_4$-capped CdSe NCs was assigned to N−H stretching vibrations from the ammonium cations. TEM images of CdSe NCs capped with Na_2MoO_4 and Na_2MoS_4 in FA showed that the NCs retained their size and monodispersity after ligand exchange (Figures 3c and S8 (SI)).

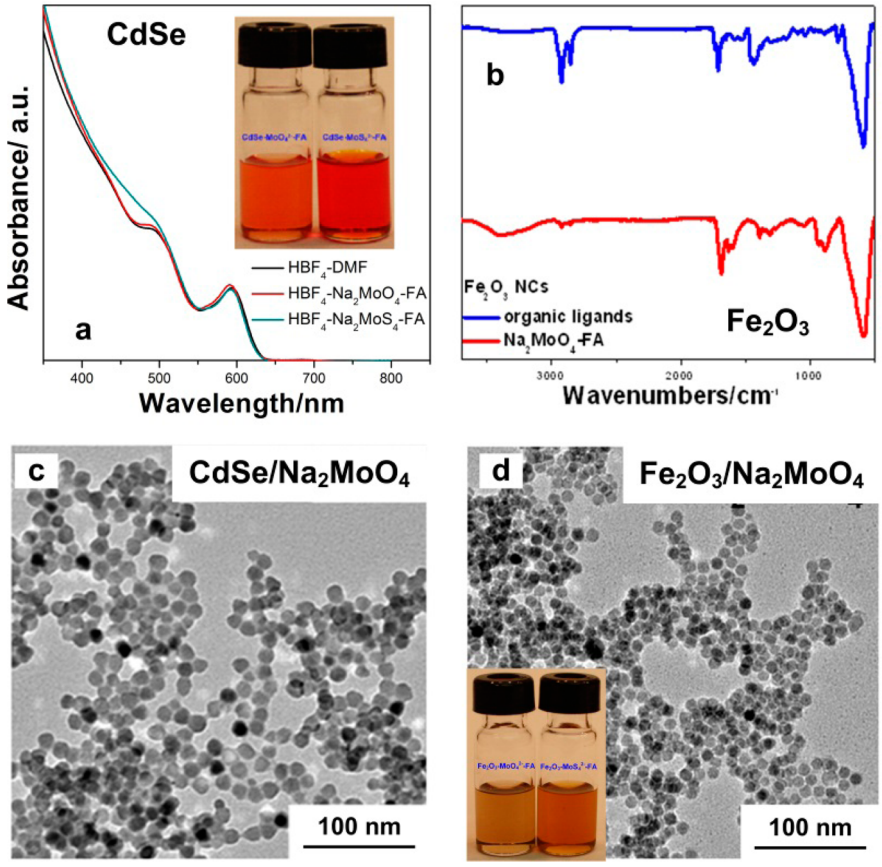

Figure 3. (a) Absorption spectra of CdSe NCs treated with HBF_4, capped with Na_2MoO_4 and Na_2MoS_4. (b) FTIR spectra of Fe_2O_3 capped with oleic acid (blue) and Na_2MoO_4 (red). (c,d) TEM images of CdSe and Fe_2O_3 capped with Na_2MoO_4, respectively.

Fe_2O_3 NCs were originally capped with OA. In the case of Fe_2O_3 NCs, MoO_4^{2-} can easily stabilize Fe_2O_3 NCs using a two-step ligand exchange under a wide range of pH, while MoS_4^{2-} only stabilized NCs after washing with acetonitrile, which increased the solution pH, as previously shown in Table 1. The inset in Figure 3d shows that MoS_4^{2-} and MoO_4^{2-}-capped Fe_2O_3 NCs formed stable colloidal solutions in FA. The FTIR spectra were normalized referring to the intensity of Fe−O absorption band at 585 cm^{-1}. It can be seen that the C−H stretching vibrations at 2700−3100 cm^{-1} coming from OA were strongly suppressed, indicating significant removal of surface organic ligands (Figure 3b).

Direct Comparison of the Binding Affinity for Oxo- and Sulfur-Based Inorganic Ligands toward CdSe and Fe_2O_3 Nanocrystals. The binding of negatively charged oxo or MCC ligands to a positively charged NC surface changes the NC charge, which can be used to probe the binding affinity of different inorganic ligands to the NC surface. With this goal in mind, we measured the electrophoretic mobilities and plotted them according to the ligand's concentration for a number of inorganic oxo- and sulfur-based ligands (Figure 4). This approach, known as ζ-potential titration, is used to measure isoelectric points for colloids and emulsions.[42] Here we used it to compare the ligand binding of different ligands to the NC surface. As discussed above, the pH of colloidal solution has a critical influence on ligand binding. The distinct difference of binding affinity of the same ligand to the same amount of Fe_2O_3 NCs at different pH values resulted in the following observations: at pH 1.8, the addition of 150 nmol Na_2MoO_4 resulted in a negligible drop of the ζ-potential, from 31.9 mV down to 29.7 mV; at pH 11, the same amount of ligands added to the identical amount of Fe_2O_3 NCs reduced the ζ-potential from 30.3 mV down to −2.1 mV. In the case of CdSe NCs, we could also see that the ligands bound stronger to the NC surface at a higher pH (Figure S9 (SI)).

Our data suggest that ζ-potential titration is a powerful technique for assessing the binding of inorganic ligands to the NC surface. For example, direct comparison of the titration curves indicated that MoS_4^{2-} had stronger binding affinity to 4 nm CdSe NCs compared to MoO_4^{2-} at different pH values (Figures 4a and S9 (SI)). At the same time, ζ-potential titration for 10 nm Fe_2O_3 NCs showed the opposite trend for the same ligand pair (Figures 4b and S10 (SI)). We consistently observed similar trends in the families of the main group oxo ligands. When the same amount of ligand was added, AsS_3^{3-} exhibited stronger binding affinity to CdSe NCs, while $HAsO_4^{2-}$ and PO_4^{3-} showed higher binding affinity to Fe_2O_3 NCs. At all

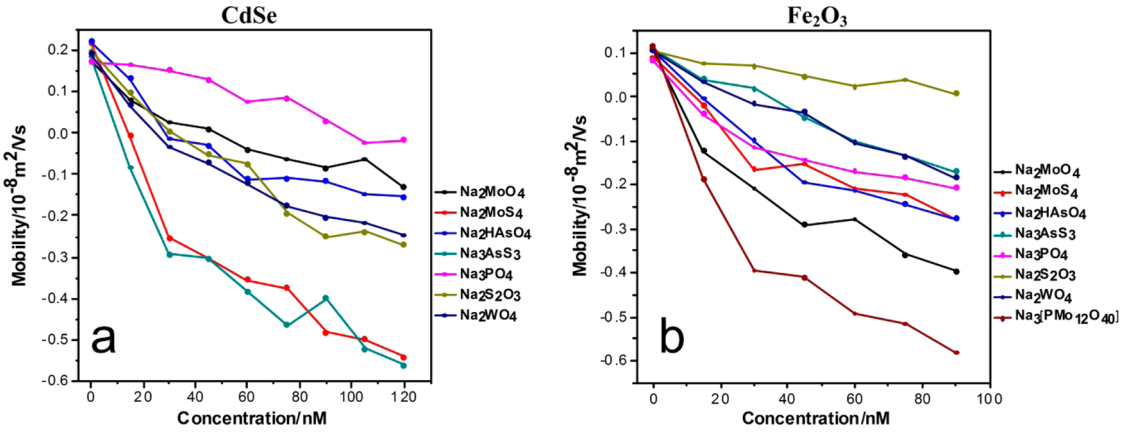

Figure 4. Electrophoretic mobility change upon addition of various oxo- and thioanions to (a) 4 nm CdSe and (b) 10 nm Fe_2O_3 NCs after ligand stripping with HBF_4 for CdSe NCs and $NOBF_4$ for Fe_2O_3 NCs, respectively.

tested pH values, chalcogenide-based ligands exhibited higher binding affinities than oxo ligands for CdSe NCs. On the contrary, oxoanions showed a much stronger binding affinity toward the Fe_2O_3 NC surface than chalcogenide-based ligands in both DMF and FA (Figure 4).

The observed trend can be explained by different chemical affinity between NCs and ligands related to the hard and soft acids and bases (HSAB) principle. We can classify Lewis acids and bases into "hard" and "soft" categories.[43] Soft acids tend to form stable complexes with soft bases while hard acids form more stable complexes with hard bases. Oxoanions are generally considered hard Lewis bases while chalcogenide-based ligands, such as AsS_3^{3-}, MoS_4^{2-}, or WS_4^{2-} are more polarizable and belong to the category of soft Lewis bases. When negatively charged ligands are added to the positively charged NC solution, they act as nucleophiles to bind to the electrophilic sites at the NC surface. For CdSe NCs, soft Cd^{2+} surface sites showed stronger affinity to soft chalcogenide-based ligands, while hard Fe^{3+} preferred binding to hard oxoanion ligands in the case of Fe_2O_3 NCs. Both oxoanion and chalcogenide-based ligands were able to stabilize CdSe or Fe_2O_3 NCs.

We conducted a similar ligand exchange procedure on III−V NCs, and the results are summarized in Table 2. We found that most of the simple oxoanions can functionalize III−V NCs easily, and InP NCs showed a relatively higher tendency for oxoanion-specific adsorption than InAs NCs. This can be also be rationalized within the HSAB principle if we take into account that the presence of soft atoms (like As, formally in −3 oxidation state in InAs) softens In^{3+} metal sites.[21]

Polyoxometallates (POMs) as Surface Ligands for Colloidal NCs. POMs are inorganic metal−oxygen cluster anions consisting of three or more transition metal oxoanions linked together by shared oxygen atoms. These heavily charged anions can accept several electrons without significant structural changes. The delocalization of these electrons within the POM framework makes them important species for catalysis and related applications. The Finke group demonstrated POM's capability for stabilizing colloidal solutions of metal NCs.[28−31] Recently, the Milliron group developed *ex situ* and *in situ* ligand exchange procedures to convert ITO NCs into metal oxide composite films using POMs ($[Nb_6O_{19}]^{8-}$, $[VO_2(C_2O_4)_2]^{3-}$) as the exchanging ligands.[27,44] Here we explored the ligand chemistry of POMs with early transition metals, molybdenum or tungsten on metal oxide NCs (Fe_2O_3, ZnO, $CoFe_2O_4$, TiO_2), and semiconductor NCs (InP). Most Keggin type POMs $[X^{n+}M_{12}O_{40}]^{(8-n)-}$ used in this work were commercially available (X = P, Si; M = Mo, W). We also prepared Dawson type POMs $[(X^{n+})_2M_{18}O_{62}]^{(16-2n)-}$, polymolybdate giant wheels $Na_{21}[Mo_{126}^{VI}Mo_{28}^{V}O_{462}H_{14}(H_2O)_{54}(H_2PO_2)_7]$ (Figure S11 (SI)), and the known water oxidation catalyst $Rb_8K_2[\{Ru_4O_4(OH)_2(H_2O)_4\}(\gamma\text{-}SiW_{10}O_{36})_2]\cdot 25H_2O$ following the literature.[45,46]

The two-step ligand exchange procedure has been used to replace the original organic ligands with POMs as described above. As in the case of Fe_2O_3 NCs, other metal oxide NCs including ZnO, $CoFe_2O_4$, and TiO_2 were all able to form colloidally stable solutions in DMF with positively charged surfaces using ligand-stripping agents. They were further mixed with negatively charged POMs to obtain colloidal stability in FA. Metal oxide NC that formed a stable colloidal solution with corresponding POMs in FA are summarized in Table 3. Some POMs could not instantaneously stabilize NCs, instead taking a few hours to reach stabilization. Gentle heating usually accelerated the ligand's dynamics in solution, thereby reaching equilibrium faster.

The POM-capped Fe_2O_3 NCs were highly stable in formamide. TEM images of Fe_2O_3 NCs capped with $Na_3[PW_{12}O_{40}]$ and $K_6[P_2W_{18}O_{62}]$ showed NCs that retained their size and monodispersity after ligand exchange (Figures 5a and S12 (SI)). Dynamic light scattering measurements also confirmed that Fe_2O_3

TABLE 3. Colloidal Stability of Metal oxide NCs Capped with Polyoxometallates[a]

ligands	Fe_2O_3	ZnO	$CoFe_2O_4$	TiO_2
$H_3[PMo_{12}O_{40}]$	+			+
$H_3[PW_{12}O_{40}]$	+			+
$Na_3PMo_{12}O_{40}$	+			+
$Na_6H_2W_{12}O_{40}$	+			+
$H_4[SiW_{12}O_{40}]$	+			
$K_6[P_2W_{18}O_{62}]$	+	+	+	+
$K_6[P_2Mo_{18}O_{62}]$	+		+	+
$Na_{21}[Mo_{126}^{VI}Mo_{28}^{V}O_{462}H_{14}(H_2O)_{54}(H_2PO_2)_7]$	+		+	+
$Rb_8K_2[\{Ru_4O_4(OH)_2(H_2O)_4\}(\gamma\text{-}SiW_{10}O_{36})_2]$	+			

[a] "+" corresponds to ability of particular NCs to form stable colloidal solution with a given oxo ligand. "—" corresponds to failed attempts to form stable colloids. The NC solution was considered stable if the solution was optically clear and did not form precipitate after a few weeks or under centrifugation.

NCs retained their monodispersity after ligand exchange with POMs. The hydrodynamic diameter of NCs decreased from 15 to 13 nm after the removal of organic ligands and increased by 1−2 nm after capping with POMs (Figure 5b), indicating the possibility of direct binding of POMs to the Fe_2O_3 NC surface. To further prove the binding of POMs to the NC surface, we carried out ^{31}P NMR measurements on Dawnson type $K_6[P_2W_{18}O_{62}]$ with the addition of positively charged ZnO NCs in FA (Figure 5c). After integration, the relative intensity of the ^{31}P signal from $K_6[P_2W_{18}O_{62}]$ referenced to the H_3PO_4 internal standard was 1, 0.34, and 0.13, respectively, with the increasing amount of added ZnO NCs. The decrease in the phosphorus peak at −12.25 ppm can be explained by the fact that free POM molecules were bound to the ZnO NC surface. We observed no change in the phosphorus chemical shift. This is because the PO_4 unit in $K_6[P_2W_{18}O_{62}]$ is surrounded by WO_8 octahedrons, which isolates phosphorus atoms making them less sensitive to the surrounding environment. This POM has a broad pH range of stability against fragmentation or hydrolysis and can be protonated only at a pH below 5.[47]

The solution ^{31}P NMR data still do not answer the question whether the POM molecules retain their integrity after binding to the NC surface. To clarify this point, we used the solid state MAS ^{31}P NMR measurements for NCs functionalized with Keggin or Dawson type POMs. As mentioned above, the intrinsic advantage of POM is that chemical shifts would remain similar (P atoms are well shielded inside the POM cluster), while signal broadening will be substantial, but measurable. Figure 5d shows the ^{31}P NMR spectra for free and surface-immobilized $K_6[P_2W_{18}O_{62}]$ on TiO_2 nanoplates. Before ligand exchange, $K_6[P_2W_{18}O_{62}]$ contained a single peak at −13.24 ppm, in full agreement with literature,[47] which can be assigned to both phosphorus atoms in POM since they have an identical environment. After ligand exchange, the spectrum exhibits two peaks at −11.18 and −14.78 ppm. As a plausible explanation, the elongated Dawson-type POM anion may be binding to the NC surface with one side, introducing an asymmetry in electronic shielding for P atoms. Even in MAS NMR, the peaks are significantly broader because line width after ligand binding can also be affected by the spread in chemical shifts due to multiple binding sites and various surface facets. Overall, these measurements confirm that Dawson-type POM was successfully immobilized on the TiO_2 nanoplate surface. Furthermore, we also studied the Keggin-type POM using NMR spectroscopy techniques (Figure S13 (SI)) and observed similar behavior.

We used ζ-potential titration to compare the binding between Fe_2O_3 NCs and POMs or small oxoanions under the same condition. Figures 4b and S10 (SI) indicate that addition of the same amount of POM results in a higher density of surface charge compared with small oxoanions like PO_4^{3-}. Given the same charge on both ions, we may conclude that POMs bind stronger to the Fe_2O_3 NC surface than small oxoanions, such as PO_4^{3-} or MoO_4^{2-}, in either DMF or FA. A possible explanation is that in addition to Coulombic interactions between the charged NC surface and POM molecules, van der Waals forces can additionally strengthen bonding between NCs and POM.

Generally, ligand exchange chemistry with POMs works easily for metal oxide NCs including Fe_2O_3, $CoFe_2O_4$, ZnO, and TiO_2 (Table 3) but not for semiconductor CdSe NCs. We could not functionalize CdSe NCs with POMs in FA either through a direct phase transfer procedure or through a two-step ligand exchange procedure. We were able to obtain stable colloidal solutions of CdSe NCs in the presence of POMs when NMF was used as the solvent, but there was no conclusive data about binding of POMs to the NC surface. Interestingly, InP NCs can be stabilized by $[PMo_{12}O_{40}]^{3-}$ POM in FA, which could be of importance because such composite combines the optical and electronic properties of semiconductor quantum dots with the catalytic properties of POMs. Generally speaking, ligand exchange with oxoanions was much easier for III−V semiconductor NCs than for II−VI NCs. It could be because In^{3+} metal sites are usually considered harder than Cd^{2+} metal sites in terms of their Lewis acidity, which suggests that In^{3+}-containing NCs should possess a higher binding affinity to oxo ligands according to the HSAB principle.

Prospective Applications of Nanocrystals Capped with Inorganic Oxo Ligands. The functionalization of nanomaterials with inorganic oxoanions, including oxometallates, opens up a number of opportunities for rational design of functional materials where physical or chemical properties of the nanocomponent are combined with the properties of the oxoanion in a synergistic manner. In this subsection we discuss two examples showing

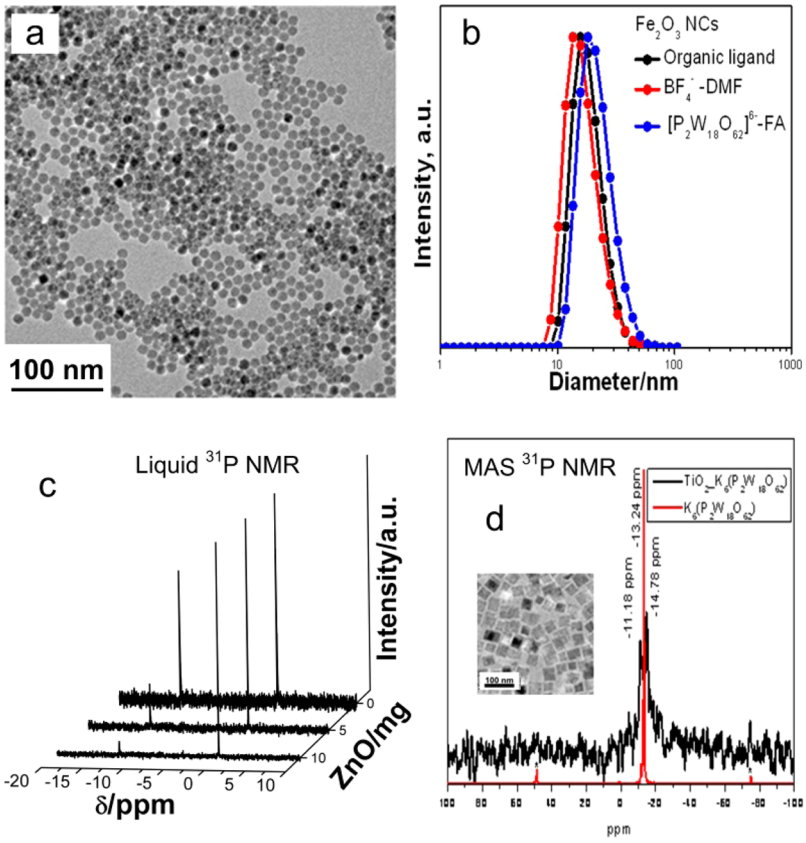

Figure 5. (a) TEM image of Fe_2O_3 NCs capped with $Na_3[PW_{12}O_{40}]$ POM. (b) The DLS curves of Fe_2O_3 NCs capped with organic ligand, bare, and with $K_6[P_2W_{18}O_{62}]$, respectively. (c) Solution ^{31}P NMR of $K_6[P_2W_{18}O_{62}]$ recorded for free POM and in the presence of different amounts of ZnO NCs, from the front to back, with H_3PO_4 as the internal standard. (d) Solid state MAS ^{31}P NMR of $K_6[P_2W_{18}O_{62}]$ and TiO_2 NCs capped with $K_6[P_2W_{18}O_{62}]$. Inset shows TEM image of TiO_2 NCs.

that inorganic oxo ligands can be used for designing functional materials from NC building blocks. In the first example, we used Fe_2O_3 NCs capped with MoO_4^{2-} ligands as the prototype cathode material for Li-ion batteries. In the second example, we attached catalytically active POM to the surface of Fe_2O_3 NCs and demonstrated electrocatalytic water oxidation at the NC surface. These examples complement the recent work by Milliron *et al.*, where indium tin oxide NCs were combined with $[N(CH_3)_4]_6[Nb_{10}O_{28}]$ POM to build a composite material with advanced electrochromic properties.[27]

Effect of MoO_4^{2-} Ligand on Li^+ Intercalation into Fe_2O_3 Nanoparticles. The functionalization of the NC surface with oxo ligands is a promising way to prepare doped nanostructures that can be used as efficient electrode material in Li^+-ion batteries. This has been demonstrated with the example of iron oxide NCs modified with MoO_4^{2-} surface ligands. These hollow NCs were prepared by first synthesizing Fe/Fe_3O_4 core–shell NCs, exchanging the original oleylamine capping molecules with MoO_4^{2-}, followed by thermal annealing at 200 °C for 12 h under ambient conditions, as shown in Figure 6. During the annealing step, core–shell NCs transformed into 14 nm hollow γ-Fe_2O_3 NCs with ~4.5 nm shells doped with molybdenum ions, as confirmed by TEM (Figure 6b), X-ray diffraction (Figure S14a (SI)), XANES (Figures 7a and S14b (SI)), and EXAFS (Figures 7b and S14c (SI)) measurements.

The oxidation of the metallic iron core took place according to the Kirkendal effect.[48,49] Most likely, incorporation of Mo ions into the γ-Fe_2O_3 hollow shell happened because of the diffusion of iron toward the interface where it oxidized. The oxidation state of molybdenum ions is close to +VI, based on the position of the absorption edge in the XANES spectrum (Figure 7a). While no change in the oxidation state of molybdenum ions takes place upon annealing, as indicated by the XANES data, the intensity of the EXAFS signal at 1.3 Å, corresponding to Mo–O correlations, significantly drops down after annealing (Figure 7b). Such change in the EXAFS pattern can be explained by the inclusion of Mo^{VI} species into the γ-Fe_2O_3 lattice. The strong XANES pre-edge peak suggests that Mo^{VI} ions preserved a tetrahedral coordination environment, presumably occupying the tetrahedral sites of the γ-Fe_2O_3 lattice.

Doping of the crystalline lattice with multivalent cations leads to the increased concentration of cation vacancies.[50] Previously, Koo *et al.* have shown that typical anode materials, such as iron oxide, can be

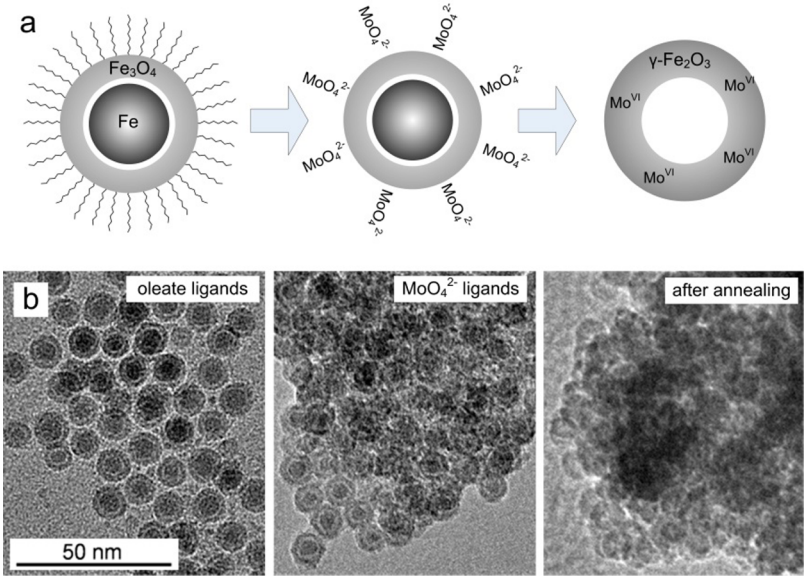

Figure 6. (a) Scheme describing the preparation of Mo^{VI}-doped γ-Fe_2O_3 hollow NCs, starting from Fe/Fe_3O_4 core–shell NCs, through the exchange of oleylamine ligands with MoO_4^{2-}, followed by annealing in air at 200 °C for 12 h to form hollow γ-Fe_2O_3 NCs *via* the Kirkendal effect. (b) TEM images of the NCs at different stages described in (a).

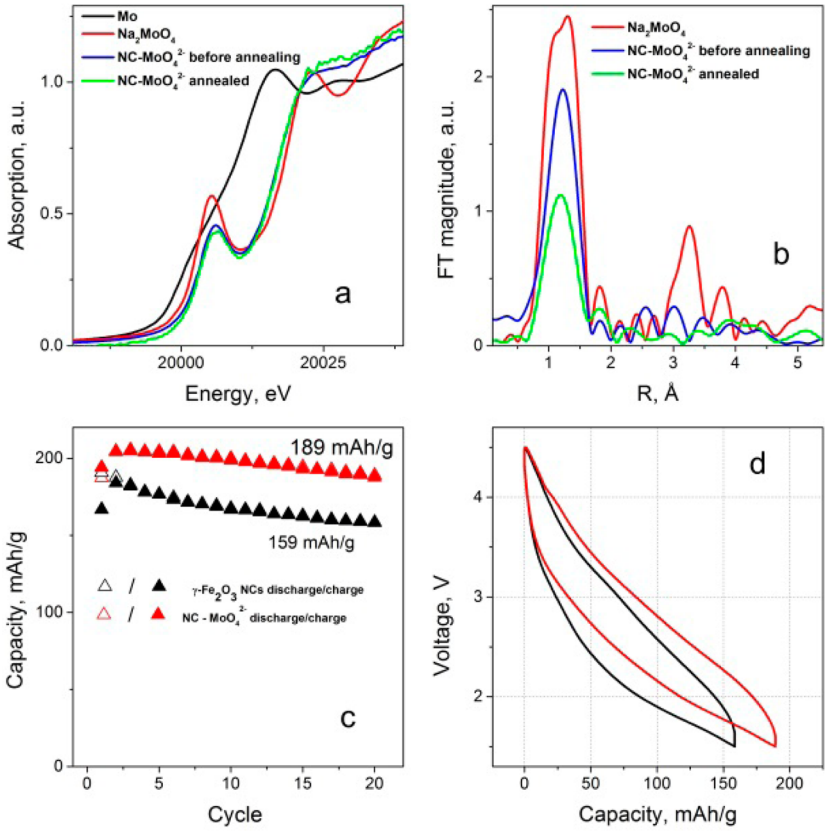

Figure 7. (a) Mo edge XANES and (b) Fourier transforms of k^2-weighted Mo edge EXAFS obtained for iron oxide NCs modified with MoO_4^{2-} before and after annealing. Bulk Na_2MoO_4 and Mo were used as references. (c) Capacity *versus* cycle number and (d) voltage profiles at the 20th intercalation/deintercalation cycle for electrodes made with hollow γ-Fe_2O_3 NCs (black line) and hollow γ-Fe_2O_3 NCs modified with MoO_4^{2-} ions (red line). The cycling current rate was 300 mA/g.

tuned into cathode materials if they contain a large concentration of cation vacancies.[51,52] Here we report that surface modification with MoO_4^{2-} ligands can be used for doping of hollow γ-Fe_2O_3 NCs with Mo^{VI+}, which stabilized vacancies in the iron sublattice. The use of MoO_4^{2-} ligands led to substantially (by ~19%) higher capacity, excellent Coulombic efficiency (~99.1%), and good capacity retention after 20

cycles (Figure 7c). Moreover, in the voltage range from 3.5 to 1.5 V, the voltage profiles of charge and discharge cycles of iron oxide NCs modified with MoO_4^{2-} are above the voltage profiles of corresponding cycles of unmodified NCs. This observation indicates that more Li ions can intercalate at higher voltages as compared with unmodified Fe_2O_3 NCs (Figure 7d). Thus, a capacity of 100 mAh/g can be obtained at 1.88 V when γ-Fe_2O_3 hollow shell NCs used as cathode materials, while the same capacity can be achieved at 2.15 V when γ-Fe_2O_3 NCs are modified with MoO_4^{2-} ligands. Therefore, surface modification with oxo ligands of multivalent elements allows the design of Li^+-ion cathode materials with higher operating voltages. In general, surface modification with oxometallate represents a promising strategy to prepare chemically doped oxide NCs.

Use of NCs Capped with POM Ligands for Electrocatalytic Water Oxidation. In the other set of experiments, we explored if POMs retained their catalytic properties after attaching to NC surfaces. Fe_2O_3 NCs were used as model metal oxide NCs with a rather low intrinsic electrocatalytic activity toward the water oxidation reaction. The NC films were deposited at the ITO surface used as a conductive substrate. Almost no catalytic activity was observed for the clean ITO electrode and the ITO electrode coated with a thin film composed of oleate-capped 10 nm Fe_2O_3 NCs. The films of organically capped Fe_2O_3 NCs showed appreciable Faradaic currents only at high overpotentials (~0.79 V), revealing the low electrocatalytic activity of Fe_2O_3 NCs (Figure S15 (SI)). The exchange of original organic ligands with Keggin-type $Na_3[PMo_{12}O_{40}]$, further referred to as "Mo-POM," resulted in significant improvements of electrocatalytic activity. The overpotential for water oxidation dropped by more than 150 mV compared to NCs capped with organic ligands (Figure S14 (SI)). Accordingly, a 65-fold increase of the exchange current density was observed upon switching to Mo-POM ligands. Both iron compounds[53,54] and molybdates[55] have shown some catalytic activity in water oxidation, but in combination they demonstrate a synergistic effect. We also synthesized $Rb_8K_2[\{Ru_4O_4(OH)_2(H_2O)_4\}(\gamma\text{-}SiW_{10}O_{36})_2]\cdot 25H_2O$, further referred to as "Ru-POM," which is known as a potent water oxidation catalyst.[46] The Fe_2O_3 NCs capped with Ru-POM showed further improvement of the electrocatalytic activity, showing *ca.* 130-fold improvement of the exchange current density compared to the original Fe_2O_3 NCs (Figure S15 (SI)). It is likely that such specially designed ligands will demonstrate even higher catalytic activity after systematic optimization. Coupling oxidatively stable catalytic ligands to the NC surface may be used for designing all-inorganic photocatalysts for artificial photosynthesis.

CONCLUSIONS AND OUTLOOK

This work enriches the family of inorganic ligands for colloidal nanostructures with various oxo, oxometallate, and polyoxometallate ions. Compared with the direct phase transfer procedure, the two-step ligand exchange procedure has proven to be a much more general approach for exchanging surface ligands. It can be applied to inorganic ligand exchange chemistry for different NCs with a variety of ligands including chalcogenide-, halide-, and oxo-based inorganic species. This study shows comparative trends in the binding affinity of different families of inorganic ligands and clarifies the important role pH plays in the ligand exchange.

Compared to chalcogenide-based inorganic ligands, oxo ligands show larger HOMO–LUMO gaps and are more oxidatively stable. They offer a new parameter space for the rational design of functional materials. Oxo ligands should facilitate integration of nanomaterials with sol–gel chemistry and ceramics. Semiconductor NCs capped with POM ligands may efficiently combine optical and electronic properties of semiconductors with catalytic properties of POMs. The proposed materials design concept can be also applied to heterogeneous catalysts. For example, iron molybdate is an industrially used catalyst for partial oxidation of methanol into formaldehyde. There are numerous examples of other multimetallic systems that contain molybdates. Among them, Bi–Mo oxides are used for selective propene oxidation and ammoxiation into acroleine and acrylonitrile, respectively. Mo–V oxides are used for oxidation of acrolein into acrylic acid. The development of oxo ligands for various NCs may introduce a viable pathway to the rational design of complex catalytic assemblies.

METHODS

Nanocrystal Synthesis. Wurtzite phase CdSe NCs with different organic capping ligands were prepared following published protocols[56–58] with minor modifications. InP and InAs NCs were synthesized by the methods described in the literature[59–61]. Iron oxide NCs, cobalt iron oxide, zinc oxide, and titanium dioxide NCs were synthesized following established recipes.[62–66]

Synthesis of POMs. Most Keggin type POMs $[X^{n+}M_{12}O_{40}]^{(8-n)-}$ are commercially available (X = P, Si; M = Mo, W). Dawson type POMs $K_6[P_2Mo_{18}O_{62}]$, $K_6[\alpha\text{-}P_2W_{18}O_{62}]$, polymolybdate giant wheels $Na_{21}[Mo_{126}^{VI}Mo_{28}^{V}O_{462}H_{14}(H_2O)_{54}(H_2PO_2)_7]$, and the water oxidation catalyst $Rb_8K_2[\{Ru_4O_4(OH)_2(H_2O)_4\}(\gamma\text{-}SiW_{10}O_{36})_2]\cdot 25H_2O$ were prepared following the literature protocols.[45,46]

Ligand Exchange. The ligand exchange process was typically carried out in air. We used both direct phase transfer and the two-step ligand exchange process. For a typical phase transfer

process, 100 mg of an oxoanion salt was first dissolved in 4 mL of FA followed by the addition of 5 mg of NCs in hexane (4 mL). The two-phase mixture was stirred vigorously until the phase transfer of NCs from the top hexane layer to bottom FA was complete. For the two-step ligand exchange process, 5 mg of NCs were first diluted with hexane to 2−3 mL, followed by the addition of 10 mg of nitrosonium tetrafluoroborate ($NOBF_4$), trimethyloxonium tetrafluoroborate ($Me_3O^+BF_4^-$), or 20 μL of tetrafluoroboric acid (HBF_4). The mixture was stirred vigorously until the NCs were completely precipitated. The NCs were collected and dispersed into fresh DMF (5 mg/mL). To functionalize NCs, 100 μL of NCs in DMF (5 mg/mL) were precipitated with 200 μL of toluene or a toluene/hexane (1:1) mixture. The precipitated NCs could be further dispersed into DMF or ACN and precipitated with toluene or FA. 1 mL of fresh FA was added to the precipitated NCs along with 40 μL of oxo ligand solution (50 mg/mL in FA or DI water). The resulting mixture may require mild sonication to obtain a stable colloidal solution.

Characterization Techniques. UV−vis spectra of CdSe NCs were collected using a Cary 5000 UV−vis−NIR spectrophotometer. Photoluminescence spectra were measured using a FluoroMax-4 spectrofluorometer (HORIBA Jobin Yvon). Transmission electron microscopy (TEM) was performed using an FEI Tecnai F30 microscope operated at 300 kV. Fourier transform infrared (FTIR) spectra were acquired using a Nicolet Nexus-670 FTIR spectrometer. ^{31}P NMR spectra were taken using a Bruker DRX 400 NMR spectrometer (9.3 T). To prepare a reference, 85% H_3PO_4 was diluted with DI water, sealed in a 3 mm glass capillary, and used as the internal standard. The capillary was put into the NMR tube with samples, and its chemical shift was set to zero. The XRD patterns were collected using a Bruker D8 diffractometer with a Cu Kα X-ray source operating at 40 kV and 40 mA and a Vantec 2000 area detector. Dynamic light scattering (DLS) and ζ-potential data were collected using Zetasizer Nano-ZS (Malvern Instruments, UK). The Magic Angle Spinning (MAS) ^{31}P NMR experiments were performed on a Bruker AMX400 Spectrometer at 300 K using 4 mm zirconia rotors and a spinning speed of 10 kHz. The spectral frequency was set at 162.02 MHz and a 2 μs pulse length was used. The relaxation delay was 10 s, and the number of scans was 1000−2000. $(NH_4)H_2PO_4$ (1 ppm relative to H_3PO_4 with δ (^{31}P) = 0 ppm) was used as a reference.

Zeta Potential Titration. CdSe or Fe_2O_3 NCs were treated with $NOBF_4$, HBF_4, or Me_3OBF_4 to remove the surface organic ligands and made a stable colloidal solution in DMF (~5 mg/mL). These NCs were positively charged due to unbound metal sites on the surface, such as Cd^{2+} or Fe^{3+}. For ζ-potential titration, 50 μL of positively charged NCs in DMF (5 mg/mL) were added to 1 mL of DMF or FA. Oxo ligand stock solutions were prepared at different concentrations, such as 3, 5, 10, and 15 mM in FA. The ζ-potential of the colloidal solution was measured with the slow addition of the oxo ligand stock solution. Typically, the positive NC surface charge was slowly neutralized and recharged by negatively charged oxo ligands until the NC surface was fully passivated, at which point the surface charge would be saturated.

The electrophoretic mobilities were measured using Zetasizer Nano-ZS. 4 mM $NaBF_4$ in DMF was added to the samples to define the ionic strength.

Electrochemical Measurements. The carbon nanotube (CNT)-based composite electrode design was used in Li^+-ion intercalation tests.[52] 4.0 mg of multiwall CNTs were dispersed into 150 mL of isopropyl alcohol (IPA) by 5 min sonication. Vacuum filtration was applied to the dispersion through the microporous polyolefin film (Celgard 2325), which also served as the separator in electrochemical tests. The black layer of the CNT was formed on the filter. Then, 12.0 mg of MoO_4^{2-}-capped γ-Fe_2O_3 NCs were combined with 3 mg of CNTs in 150 mL of IPA. The mixture was deposited onto the same filter through the same vacuum filtration procedure to form a uniform layer of active electrode material. The active layer was sealed by another CNT layer formed in the same manner as the first one. After removing the solvent residue by drying the electrode under a vacuum, the CNT-based composite electrodes were annealed in an oven at 200 °C for 12 h and used in electrochemical tests without any additional processing. No conductive additives, black carbon, or metal collector were used in the fabrication of electrodes.

The Li^+ intercalation tests were performed using 2032 coin-type cells with Li metal foil as the counter electrodes and 1.2 M $LiPF_6$ in ethylene carbonate/ethyl methyl carbonate (3:7 weight ratio) as the electrolyte (Tomiyama). Half-cell cycles were operated at 300 mA/g between 4.5−1.5 V *vs* Li/Li^+ using an automated Maccor battery tester at ambient temperature. All cell assembly and disassembly operations were performed in a He-filled dry glovebox (oxygen level <2 ppm).

EXAFS/XANES Studies. XANES (X-ray absorption near edge structure) and EXAFS (extended absorption X-ray fine structure) measurements for both the Fe K-edge (7.1 keV) and Mo K-edge (20 keV) of the NC samples were performed at the MRCAT 10-ID undulator beamline at the Advanced Photon Source (Argonne National Laboratory). Fluorescence X-rays from the samples were detected with an ion chamber placed at 45° to the incident beam. A Rh harmonic rejection mirror was used to eliminate higher energy X-rays. The gases in the ionization chamber were optimized based on the X-ray energy so that 1−5% of the X-rays were absorbed. The size of the incident X-ray beam on the sample was 0.5 mm^2. The monochromator energy was calibrated with pure Fe and Mo foils. At the MRCAT beamline, the Si(111) double crystal monochromator was scanned continuously; *i.e.*, the data was collected in quick EXAFS mode. The undulator parameters (taper and gap) were optimized to obtain a large photon flux with nearly constant intensity within the scanned energy range of 6.9−8.0 keV for the Fe K edge and 19.8−21.0 keV for the Mo K edge. Around 10 scans were recorded for each sample to ensure repeatability and averaged to improve statistics. Scattered radiation from Fe and Mo foils was measured using a pin diode during the respective Fe edge and Mo edge measurements on the samples to verify the calibration of the edge energies before merging the scans. Background subtraction, which consists of extracting the oscillations $\chi(k)$ as a function of the photoelectron wavenumber (k) from the absorption spectrum $\mu(E)$ and Fourier-transforming k-weighted $\chi(k)$ into real space $\chi(R)$, was done using the software package Athena.[67,68]

Water Oxidation Experiments. The water oxidation experiments were carried using a Gamry Reference 600 potentiostat with a three-electrode electrochemical cell. For electrochemical measurements in aqueous solutions, the pH was buffered at 6.85 by a phosphate buffer (a mixture of K_2HPO_4 and KH_2PO_4 with a total phosphate concentration of 0.05 mol/L). Glassy carbon (GC) or ITO-covered glass (ITO), platinum wire, and Ag/AgCl/(saturated KCl solution) electrodes were used as the working, counter, and reference electrodes, respectively. The NC films were prepared at the surface of working electrodes by drop casting. All solutions were carefully degassed and kept under nitrogen atmosphere.

Conflict of Interest: The authors declare no competing financial interest.

Acknowledgment. We would like to thank T. Shibata, V. Zyryanov, and C. Segre from Illinois Institute of Technology for help with EXAFS measurements and T. Shpigel for reading the manuscript. The work on synthesis and characterization of NCs was supported by the NSF under Award Number DMR-1310398 and by the NSF MRSEC Program under Award Number DMR 08-20054. Study of water oxidation was supported by the University of Chicago Institute of Molecular Engineering Water Initiative. D.V.T. thanks the David and Lucile Packard Foundation and Keck Foundation for their generous support. The work at the Center for Nanoscale Materials and the Advanced Photon Source at Argonne National Laboratory was supported by the US Department of Energy (DOE) Office of Science under Contract No. DE-AC02-06CH11357. MRCAT Beamline operations were supported by the Department of Energy and the MRCAT member institutions. M.V.K. thanks the European Union for financial support *via* ERC Starting Grant 2012 (Project NANOSOLID, GA No. 306733).

Supporting Information Available: Additional experimental details, figures, and tables. This material is available free of charge *via* the Internet at http://pubs.acs.org.

REFERENCES AND NOTES

1. Murray, C. B.; Kagan, C. R.; Bawendi, M. G. Synthesis and Characterization of Monodisperse Nanocrystals and Close-Packed Nanocrystal Assemblies. *Annu. Rev. Mater. Sci.* **2000**, *30*, 545.
2. Ghosh Chaudhuri, R.; Paria, S. Core/Shell Nanoparticles: Classes, Properties, Synthesis Mechanisms, Characterization, and Applications. *Chem. Rev.* **2012**, *112*, 2373–2433.
3. Laurent, S.; Forge, D.; Port, M.; Roch, A.; Robic, C.; Vander Elst, L.; Muller, R. N. Magnetic Iron Oxide Nanoparticles: Synthesis, Stabilization, Vectorization, Physicochemical Characterizations, and Biological Applications. *Chem. Rev.* **2008**, *108*, 2064–2110.
4. Sun, Y.; Xia, Y. Shape-Controlled Synthesis of Gold and Silver Nanoparticles. *Science* **2002**, *298*, 2176–2179.
5. Manna, L.; Scher, E. C.; Alivisatos, A. P. Synthesis of Soluble and Processable Rod-, Arrow-, Teardrop-, and Tetrapod-Shaped CdSe Nanocrystals. *J. Am. Chem. Soc.* **2000**, *122*, 12700–12706.
6. Huang, J.; Kovalenko, M. V.; Talapin, D. V. Alkyl Chains of Surface Ligands Affect Polytypism of CdSe Nanocrystals and Play an Important Role in the Synthesis of Anisotropic Nanoheterostructures. *J. Am. Chem. Soc.* **2010**, *132*, 15866–15868.
7. Burda, C.; Chen, X.; Narayanan, R.; El-Sayed, M. A. Chemistry and Properties of Nanocrystals of Different Shapes. *Chem. Rev.* **2005**, *105*, 1025–1102.
8. Mokari, T.; Rothenberg, E.; Popov, I.; Costi, R.; Banin, U. Selective Growth of Metal Tips onto Semiconductor Quantum Rods and Tetrapods. *Science* **2004**, *304*, 1787–1790.
9. Talapin, D. V.; Nelson, J. H.; Shevchenko, E. V.; Aloni, S.; Sadtler, B.; Alivisatos, A. P. Seeded Growth of Highly Luminescent CdSe/CdS Nanoheterostructures with Rod and Tetrapod Morphologies. *Nano Lett.* **2007**, *7*, 2951–2959.
10. Drndic, M.; Jarosz, M. V.; Morgan, N. Y.; Kastner, M. A.; Bawendi, M. G. Transport Properties of Annealed CdSe Colloidal Nanocrystal Solids. *J. Appl. Phys.* **2002**, *92*, 7498–7503.
11. Shim, M.; Guyot-Sionnest, P. N-Type Colloidal Semiconductor Nanocrystals. *Nature* **2000**, *407*, 981–983.
12. Kovalenko, M. V.; Scheele, M.; Talapin, D. V. Colloidal Nanocrystals with Molecular Metal Chalcogenide Surface Ligands. *Science* **2009**, *324*, 1417–1420.
13. Lee, J.-S.; Kovalenko, M. V.; Huang, J.; Chung, D. S.; Talapin, D. V. Band-Like Transport, High Electron Mobility and High Photoconductivity in All-Inorganic Nanocrystal Arrays. *Nat. Nanotechnol.* **2011**, *6*, 348–352.
14. Liu, W.; Lee, J.-S.; Talapin, D. V. III-V Nanocrystals Capped with Molecular Metal Chalcogenide Ligands: High Electron Mobility and Ambipolar Photoresponse. *J. Am. Chem. Soc.* **2013**, *135*, 1349–1357.
15. Choi, J.-H.; Fafarman, A. T.; Oh, S. J.; Ko, D.-K.; Kim, D. K.; Diroll, B. T.; Muramoto, S.; Gillen, J. G.; Murray, C. B.; Kagan, C. R. Bandlike Transport in Strongly Coupled and Doped Quantum Dot Solids: A Route to High-Performance Thin-Film Electronics. *Nano Lett.* **2012**, *12*, 2631–2638.
16. Kovalenko, M. V.; Spokoyny, B.; Lee, J.-S.; Scheele, M.; Weber, A.; Perera, S.; Landry, D.; Talapin, D. V. Semiconductor Nanocrystals Functionalized with Antimony Telluride Zintl Ions for Nanostructured Thermoelectrics. *J. Am. Chem. Soc.* **2010**, *132*, 6686–6695.
17. Liu, Y.; Tolentino, J.; Gibbs, M.; Ihly, R.; Perkins, C. L.; Liu, Y.; Crawford, N.; Hemminger, J. C.; Law, M. PbSe Quantum Dot Field-Effect Transistors with Air-Stable Electron Mobilities above 7 $cm^2 V^{-1} s^{-1}$. *Nano Lett.* **2013**, *13*, 1578–1587.
18. Kim, D. K.; Lai, Y. M.; Diroll, B. T.; Murray, C. B.; Kagan, C. R. Flexible and Low-Voltage Integrated Circuits Constructed from High-Performance Nanocrystal Transistors. *Nat. Commun.* **2012**, 3.
19. Son, J. S.; Zhang, H.; Jang, J.; Poudel, B.; Waring, A.; Nally, L.; Talapin, D. V. All-Inorganic Nanocrystals as a Glue for BiSbTe Grains: Design of Interfaces in Mesostructured Thermoelectric Materials. *Angew. Chem., Int. Ed.* **2014**, *53*, 7466–7470.
20. Kovalenko, M. V.; Schaller, R. D.; Jarzab, D.; Loi, M. A.; Talapin, D. V. Inorganically Functionalized PbS/CdS Colloidal Nanocrystals: Integration into Amorphous Chalcogenide Glass and Luminescent Properties. *J. Am. Chem. Soc.* **2012**, *134*, 2457–2460.
21. Nag, A.; Kovalenko, M. V.; Lee, J.-S.; Liu, W.; Spokoyny, B.; Talapin, D. V. Metal-Free Inorganic Ligands for Colloidal Nanocrystals: S^{2-}, HS^-, Se^{2-}, HSe^-, Te^{2-}, HTe^-, TeS_3^{2-}, OH^- and NH_2^- as Surface Ligands. *J. Am. Chem. Soc.* **2011**, *133*, 10612–10620.
22. Fafarman, A. T.; Koh, W.-k.; Diroll, B. T.; Kim, D. K.; Ko, D.-K.; Oh, S. J.; Ye, X.; Doan-Nguyen, V.; Crump, M. R.; Reifsnyder, D. C.; *et al.* Thiocyanate-Capped Nanocrystal Colloids: Vibrational Reporter of Surface Chemistry and Solution-Based Route to Enhanced Coupling in Nanocrystal Solids. *J. Am. Chem. Soc.* **2011**, *133*, 15753–15761.
23. Dirin, D. N.; Dreyfuss, S.; Bodnarchuk, M. I.; Nedelcu, G.; Papagiorgis, P.; Itskos, G.; Kovalenko, M. V. Lead Halide Perovskites and Other Metal Halide Complexes as Inorganic Capping Ligands for Colloidal Nanocrystals. *J. Am. Chem. Soc.* **2014**, *136*, 6550–6553.
24. Zhang, H.; Jang, J.; Liu, W.; Talapin, D. V. Colloidal Nanocrystals with Inorganic Halide, Pseudohalide, and Halometallate Ligands. *ACS Nano* **2014**, *8*, 7359–7369.
25. Dong, A.; Ye, X.; Chen, J.; Kang, Y.; Gordon, T.; Kikkawa, J. M.; Murray, C. B. A Generalized Ligand-Exchange Strategy Enabling Sequential Surface Functionalization of Colloidal Nanocrystals. *J. Am. Chem. Soc.* **2010**, *133*, 998–1006.
26. Rosen, E. L.; Buonsanti, R.; Llordes, A.; Sawvel, A. M.; Milliron, D. J.; Helms, B. A. Exceptionally Mild Reactive Stripping of Native Ligands from Nanocrystal Surfaces by Using Meerwein's Salt. *Angew. Chem., Int. Ed.* **2011**, *51*, 684–689.
27. Llordes, A.; Garcia, G.; Gazquez, J.; Milliron, D. J. Tunable Near-Infrared and Visible-Light Transmittance in Nanocrystal-in-Glass Composites. *Nature* **2013**, *500*, 323–326.
28. Lin, Y.; Finke, R. G. Novel Polyoxoanion- and Bu_4N^+-Stabilized, Isolable, and Redissolvable, 20−30-Angstrom $Ir_{300-900}$ Nanoclusters: The Kinetically Controlled Synthesis, Characterization, and Mechanism of Formation of Organic Solvent-Soluble, Reproducible Size, and Reproducible Catalytic Activity Metal Nanoclusters. *J. Am. Chem. Soc.* **1994**, *116*, 8335–8353.
29. Watzky, M. A.; Finke, R. G. Transition Metal Nanocluster Formation Kinetic and Mechanistic Studies. A New Mechanism When Hydrogen is the Reductant: Slow, Continuous Nucleation and Fast Autocatalytic Surface Growth. *J. Am. Chem. Soc.* **1997**, *119*, 10382–10400.
30. Aiken, J. D.; Finke, R. G. Polyoxoanion- and Tetrabutylammonium-Stabilized Rh(0)n Nanoclusters: Unprecedented Nanocluster Catalytic Lifetime in Solution. *J. Am. Chem. Soc.* **1999**, *121*, 8803–8810.
31. Özkar, S.; Finke, R. G. Nanocluster Formation and Stabilization Fundamental Studies: Ranking Commonly Employed Anionic Stabilizers *via* the Development, Then Application, of Five Comparative Criteria. *J. Am. Chem. Soc.* **2002**, *124*, 5796–5810.
32. Knopf, I.; Ono, T.; Temprado, M.; Tofan, D.; Cummins, C. C. Uptake of One and Two Molecules of CO_2 by the Molybdate Dianion: a Soluble, Molecular Oxide Model System for Carbon Dioxide Fixation. *Chem. Sci.* **2014**, *5*, 1772–1776.
33. Kovalenko, M. V.; Bodnarchuk, M. I.; Zaumseil, J.; Lee, J. S.; Talapin, D. V. Expanding the Chemical Versatility of Colloidal Nanocrystals Capped with Molecular Metal Chalcogenide Ligands. *J. Am. Chem. Soc.* **2010**, *132*, 10085–10092.
34. Izumi, Y. Catalytic Beckmann Rearrangement of Oximes in Homogeneous Liquid Phase. *Chem. Lett.* **1990**, 2171–2174.
35. Holmes, R. R. Comparison of Phosphorus and Silicon: Hypervalency, Stereochemistry, and Reactivity. *Chem. Rev.* **1996**, *96*, 927–950.

36. Krossing, I.; Raabe, I. Noncoordinating Anions—Fact or Fiction? A Survey of Likely Candidates. *Angew. Chem., Int. Ed.* **2004**, *43*, 2066–2090.
37. Izutsu, K. *Electrochemistry in Nonaqueous Solutions*; Wiley-VCH: Weinheim, 2009; p xvi, 415.
38. Kallay, N. *Interfacial Dynamics*; M. Dekker: New York, 2000; p 741.
39. Kovalenko, M. V.; Bodnarchuk, M. I.; Talapin, D. V. Nanocrystal Superlattices with Thermally Degradable Hybrid Inorganic-Organic Capping Ligands. *J. Am. Chem. Soc.* **2010**, *132*, 15124–15126.
40. Tomaselli, M.; Yarger, J. L.; Bruchez, M., Jr.; Havlin, R. H.; deGraw, D.; Pines, A.; Alivisatos, A. P. NMR Study of InP Quantum Dots: Surface Structure and Size Effects. *J. Chem. Phys.* **1999**, *110*, 8861–8864.
41. Berrettini, M. G.; Braun, G.; Hu, J. G.; Strouse, G. F. NMR Analysis of Surfaces and Interfaces in 2-nm CdSe. *J. Am. Chem. Soc.* **2004**, *126*, 7063–7070.
42. Dukhin, A. S.; Goetz, P. J. Chapter 2. Fundamentals of Interface and Colloid Science. In *Studies in Interface Science*; Elsevier: Amsterdam, 2002; Vol. 15, pp 17−73.
43. Pearson, R. G. Hard and Soft Acids and Bases. *J. Am. Chem. Soc.* **1963**, *85*, 3533–3569.
44. Llordes, A.; Hammack, A. T.; Buonsanti, R.; Tangirala, R.; Aloni, S.; Helms, B. A.; Milliron, D. J. Polyoxometalates and Colloidal Nanocrystals as Building Blocks for Metal Oxide Nanocomposite Films. *J. Mater. Chem.* **2011**, *21*, 11631–11638.
45. Graham, C. R.; Finke, R. G. The Classic Wells−Dawson Polyoxometalate, $K_6[\alpha\text{-}P_2W_{18}O_{62}]\cdot 14H_2O$. Answering an 88 Year-Old Question: What is Its Preferred, Optimum Synthesis? *Inorg. Chem.* **2008**, *47*, 3679–3686.
46. Geletii, Y. V.; Botar, B.; Kögerler, P.; Hillesheim, D. A.; Musaev, D. G.; Hill, C. L. An All-Inorganic, Stable, and Highly Active Tetraruthenium Homogeneous Catalyst for Water Oxidation. *Angew. Chem., Int. Ed.* **2008**, *47*, 3896–3899.
47. Nomiya, K.; Torii, H.; Hasegawa, T.; Nemoto, Y.; Nomura, K.; Hashino, K.; Uchida, M.; Kato, Y.; Shimizu, K.; Oda, M. Insulin Mimetic Effect of a Tungstate Cluster. Effect of Oral Administration of Homo-Polyoxotungstates and Vanadium-Substituted Polyoxotungstates on Blood Glucose Level of STZ Mice. *J. Inorg. Biochem.* **2001**, *86*, 657–667.
48. Yin, Y.; Rioux, R. M.; Erdonmez, C. K.; Hughes, S.; Somorjai, G. A.; Alivisatos, A. P. Formation of Hollow Nanocrystals Through the Nanoscale Kirkendall Effect. *Science* **2004**, *304*, 711–714.
49. Cabot, A.; Puntes, V. F.; Shevchenko, E.; Yin, Y.; Balcells, L.; Marcus, M. A.; Hughes, S. M.; Alivisatos, A. P. Vacancy Coalescence during Oxidation of Iron Nanoparticles. *J. Am. Chem. Soc.* **2007**, *129*, 10358–10360.
50. Hahn, B. P.; Long, J. W.; Rolison, D. R. Something from Nothing: Enhancing Electrochemical Charge Storage with Cation Vacancies. *Acc. Chem. Res.* **2013**, *46*, 1181–1191.
51. Koo, B.; Xiong, H.; Slater, M. D.; Prakapenka, V. B.; Baasubramanian, M.; Podsiadlo, P.; Johnson, C. S.; Rajh, T.; Shevchenko, E. V. Hollow Iron Oxide Nanoparticles for Application in Lithium Ion Batteries. *Nano Lett.* **2012**, *12*, 2429–2435.
52. Koo, B.; Chattopadhyay, S.; Shibata, T.; Prakapenka, V. B.; Johnson, C. S.; Rajh, T.; Shevchenko, E. V. Intercalation of Sodium Ions into Hollow Iron Oxide Nanoparticles. *Chem. Mater.* **2013**, *25*, 245–252.
53. Ellis, W. C.; McDaniel, N. D.; Bernhard, S.; Collins, T. J. Fast Water Oxidation Using Iron. *J. Am. Chem. Soc.* **2010**, *132*, 10990–10991.
54. Fillol, J. L.; Codolà, Z.; Garcia-Bosch, I.; Gómez, L.; Pla, J. J.; Costas, M. Efficient Water Oxidation Catalysts Based on Readily Available Iron Coordination Complexes. *Nat. Chem.* **2011**, *3*, 807–813.
55. Tanaka, S.; Annaka, M.; Sakai, K. Visible Light-Induced Water Oxidation Catalyzed by Molybdenum-Based Polyoxometalates with Mono- and Dicobalt(iii) Cores as Oxygen-Evolving Centers. *Chem. Commun.* **2012**, *48*, 1653–1655.
56. Mahler, B.; Lequeux, N.; Dubertret, B. Ligand-Controlled Polytypism of Thick-Shell CdSe/CdS Nanocrystals. *J. Am. Chem. Soc.* **2009**, *132*, 953–959.
57. Carbone, L.; Nobile, C.; De Giorgi, M.; Sala, F. D.; Morello, G.; Pompa, P.; Hytch, M.; Snoeck, E.; Fiore, A.; Franchini, I. R.; *et al.* Synthesis and Micrometer-Scale Assembly of Colloidal CdSe/CdS Nanorods Prepared by a Seeded Growth Approach. *Nano Lett.* **2007**, *7*, 2942–2950.
58. Chen, O.; Chen, X.; Yang, Y.; Lynch, J.; Wu, H.; Zhuang, J.; Cao, Y. C. Synthesis of Metal−Selenide Nanocrystals Using Selenium Dioxide as the Selenium Precursor. *Angew. Chem., Int. Ed.* **2008**, *47*, 8638–8641.
59. Micic, O. I.; Curtis, C. J.; Jones, K. M.; Sprague, J. R.; Nozik, A. J. Synthesis and Characterization of InP Quantum Dots. *J. Phys. Chem.* **1994**, *98*, 4966–4969.
60. Battaglia, D.; Peng, X. Formation of High Quality InP and InAs Nanocrystals in a Noncoordinating Solvent. *Nano Lett.* **2002**, *2*, 1027–1030.
61. Guzelian, A. A.; Banin, U.; Kadavanich, A. V.; Peng, X.; Alivisatos, A. P. Colloidal Chemical Synthesis and Characterization of InAs Nanocrystal Quantum Dots. *Appl. Phys. Lett.* **1996**, *69*, 1432–1434.
62. Kovalenko, M. V.; Bodnarchuk, M. I.; Lechner, R. T.; Hesser, G.; Schaffler, F.; Heiss, W. Fatty Acid Salts as Stabilizers in Size- and Shape-Controlled Nanocrystal Synthesis: The Case of Inverse Spinel Iron Oxide. *J. Am. Chem. Soc.* **2007**, *129*, 6352–6355.
63. Chen, Y.; Kim, M.; Lian, G.; Johnson, M. B.; Peng, X. Side Reactions in Controlling the Quality, Yield, and Stability of High Quality Colloidal Nanocrystals. *J. Am. Chem. Soc.* **2005**, *127*, 13331–13337.
64. Wang, H. Z.; Si, H. L.; Zhao, H. L.; Du, Z. L.; Li, L. S. Shape-Controlled Synthesis of Cobalt Oxide Nanocrystals Using Cobalt Acetylacetonate. *Mater. Lett.* **2010**, *64*, 408–410.
65. Gordon, T. R.; Cargnello, M.; Paik, T.; Mangolini, F.; Weber, R. T.; Fornasiero, P.; Murray, C. B. Nonaqueous Synthesis of TiO_2 Nanocrystals Using TiF_4 to Engineer Morphology, Oxygen Vacancy Concentration, and Photocatalytic Activity. *J. Am. Chem. Soc.* **2012**, *134*, 6751–6761.
66. Bodnarchuk, M. I.; Kovalenko, M. V.; Groiss, H.; Resel, R.; Reissner, M.; Hesser, G.; Lechner, R. T.; Steiner, W.; Schäffler, F.; Heiss, W. Exchange-Coupled Bimagnetic Wüstite/Metal Ferrite Core/Shell Nanocrystals: Size, Shape, and Compositional Control. *Small* **2009**, *5*, 2247–2252.
67. Newville, M. IFEFFIT: Interactive EXAFS Analysis and FEFF Fitting. *J. Synchrotron Radiat.* **2001**, *8*, 322–324.
68. Ravel, B.; Newville, M. ATHENA, ARTEMIS, HEPHAESTUS: Data Analysis for X-Ray Absorption Spectroscopy Using IFEFFIT. *J. Synchrotron Radiat.* **2005**, *12*, 537–541.